

Research Article

Complex Wavelet Transform-Based Face Recognition

Alaa Eleyan, Hüseyin Özkaramanli, and Hasan Demirel

Electrical & Electronic Engineering Department, Eastern Mediterranean University, Famagusta, Northern Cyprus, 10-Mersin, Turkey

Correspondence should be addressed to Alaa Eleyan, alaa.eleyan@emu.edu.tr

Received 1 September 2008; Accepted 19 December 2008

Recommended by João Manuel R. S. Tavares

Complex approximately analytic wavelets provide a local multiscale description of images with good directional selectivity and invariance to shifts and in-plane rotations. Similar to Gabor wavelets, they are insensitive to illumination variations and facial expression changes. The complex wavelet transform is, however, less redundant and computationally efficient. In this paper, we first construct complex approximately analytic wavelets in the single-tree context, which possess Gabor-like characteristics. We, then, investigate the recently developed dual-tree complex wavelet transform (DT-CWT) and the single-tree complex wavelet transform (ST-CWT) for the face recognition problem. Extensive experiments are carried out on standard databases. The resulting complex wavelet-based feature vectors are as discriminating as the Gabor wavelet-derived features and at the same time are of lower dimension when compared with that of Gabor wavelets. In all experiments, on two well-known databases, namely, FERET and ORL databases, complex wavelets equaled or surpassed the performance of Gabor wavelets in recognition rate when equal number of orientations and scales is used. These findings indicate that complex wavelets can provide a successful alternative to Gabor wavelets for face recognition.

Copyright © 2008 Alaa Eleyan et al. This is an open access article distributed under the Creative Commons Attribution License, which permits unrestricted use, distribution, and reproduction in any medium, provided the original work is properly cited.

1. INTRODUCTION

Identifying a person using geometric or statistical features derived from a face image is an important and challenging task [1–3]. This task becomes even more challenging due to the fact that large variations in the visual stimulus arising from illumination condition, viewing directions, poses, facial expression, aging, disguises are all common in real applications. A face recognition system should, to a large extent, take into account all the above-mentioned natural constraints and cope with them in an effective manner. In order to achieve this, one must have efficient and effective representations for faces. It is important that the representation of face images have the following desirable properties. (1) It should require minimum or no manual annotations, so that the face recognition task can be performed automatically; (2) representation should not be redundant. In other words, the feature vector representing the face image should contain critical amount of information in order to make sure that the dimensionality of the representation is minimal; (3) the representation should cope satisfactorily with the nonideal effects such as illumination variations, pose, aging, facial expression, and partial occlusions; (4) invariance to shifts,

in-plane rotations; (5) directional selectivity in many scales; (6) low-computational complexity. Furthermore, it is also desirable that the representation derives its roots in some form from the principles of human visual processing.

Many techniques have been proposed in the literature for representing face images. Some of these include principal components analysis [2–4], discrete wavelet transform [5, 6], and discrete cosine transform [7].

Gabor wavelet-based representation provides an excellent solution when one considers all the above desirable properties. For this reason, Gabor wavelets have been extensively studied in many image processing applications [8–11].

Lades et al. [12] used a dynamic link architecture framework of the Gabor wavelet for face recognition. Wiskott et al. [13] subsequently developed a Gabor wavelet-based elastic bunch graph matching (EBGM) method to label and recognize human faces. Zhang et al. [14] introduced an object descriptor based on histogram of Gabor phase pattern for face recognition. Liu et al. [15] proposed a method to determine the optimal position for extracting the Gabor feature such that the number of feature points is minimized while the representation capability is maximized.

Liu and Wechsler [16] presented an independent Gabor features (IGFs) method based on the independent component analysis [17]. For extensive review of invariant properties of Gabor wavelets and their application to face recognition using Gabor wavelets, one is referred to [18–20].

Even though Gabor wavelet-based face image representation is optimal in many respects, it has got two important drawbacks that shadow its success. First, it is computationally very complex. A full representation encompassing many directions (e.g., 8 directions), and many scales (e.g., 5 scales) requires the convolution of the face image with 40 Gabor wavelet kernels.

Second, memory requirements for storing Gabor features are very high. The size of the Gabor feature vector for an input image of size 128×128 pixels is $128 \times 128 \times 40 = 655360$ pixels when the representation uses 8 directions and 5 scales.

There have been many research works which try to alleviate the above problems by using weighted sub-Gabor [21], simplified Gabor wavelets [22], optimal sampling of Gabor features [15], and so forth. None of these attempts, however, approaches the problem in a structured fashion and therefore in most cases it is questionable whether the desirable properties of the Gabor representation is preserved as a result of the respective approach used.

Complex approximately analytic wavelets provide a multiscale representation of images with good directional selectivity, invariance to shifts and in-plane rotation, and phase information much like the Gabor wavelets. The complex wavelets, however, are orthogonal and can be implemented with short one-dimensional separable filters which make them computationally very attractive. Unlike the Gabor wavelets, where the redundancy is 40 times with 5 scales and 8 directions, complex wavelet representation is 4 times redundant in 2 dimensions and the redundancy is independent of the number of scales used. Thus, complex approximately analytic wavelets provide an excellent alternative to Gabor wavelets with the potential to overcome the above-mentioned shortcomings of the Gabor wavelets. Sankaran et al. [23] and Celik et al. [24] used the DT-CWT and Gabor wavelets for facial feature extraction, where in both papers authors report comparable performance of the DT-CWT with more efficient computational complexity. In [25], Sun and Du applied DT-CWT on spectral histogram PCA space for face detection. In [26, 27], the authors used orthogonal neighborhood preserving projections (ONPPs) and supervised kernel ONPP with DT-CWT for face recognition. Their preliminary results indicate that KONPP produce superior performance.

In this paper, we systematically study complex wavelets for the face recognition problem. Specifically, we employ the recently developed dual-tree complex wavelet transform and a new single-tree complex wavelet transform with improved shift invariance and directional selectivity properties. First, Gabor wavelet and complex wavelet-based representations of face images are obtained. For all the transforms, the representations encompass 4 levels and 6 directions. PCA is employed to further reduce the dimensionality of the derived feature vectors. Finally, 3 types of similarity measures used for identification. Results of experiments carried out on

FERET and ORL databases indicate that complex wavelets indeed constitute an excellent alternative to Gabor wavelets in face image representation and recognition.

The rest of the paper is organized as follows. Sections 2 and 3 briefly give an overview of Gabor wavelets, DT-CWT, and ST-CWT. Section 4 describes the proposed method, and Section 5 discusses the simulation results. Computational complexity analysis for feature extraction can be found in Section 6.

2. GABOR WAVELETS

A Gabor wavelet filter is a Gaussian kernel function modulated by a sinusoidal plane wave:

$$\begin{aligned} \psi_g(x, y) &= \frac{f^2}{\eta\gamma\pi} \exp(\beta^2 y'^2 - \alpha^2 x'^2) \exp(2\pi j f x'), \\ x' &= x \cos \theta + y \sin \theta, \\ y' &= y \cos \theta - x \sin \theta, \end{aligned} \quad (1)$$

where f is the central frequency of the sinusoidal plane wave, θ is the anticlockwise rotation of the Gaussian and the envelope wave, α is the sharpness of the Gaussian along the major axis parallel to the wave, and β is the sharpness of the Gaussian minor axis perpendicular to the wave. $\gamma = f/\alpha$ and $\eta = f/\beta$ are defined to keep the ratio between frequency and sharpness constant [8]. The 2D Gabor wavelet as defined in (1) has Fourier transform:

$$\begin{aligned} \Psi_g(u, v) &= \exp\left(-\pi^2 \left(\frac{(u' - f)^2}{\alpha^2} + \frac{v'^2}{\beta^2}\right)\right), \\ u' &= u \cos \theta + v \sin \theta, \\ v' &= v \cos \theta - u \sin \theta. \end{aligned} \quad (2)$$

Figures 1(a) and 1(b) show, respectively, the real part and magnitude of the Gabor wavelets for 4 scales and 6 directions. Figure 2 shows the 1D Gabor wavelets in the frequency domain. At all levels, the wavelet is a Gaussian bandpass filter.

Gabor wavelets possess many properties which make them attractive for many applications. Directional selectivity is one of the most important of these properties. The Gabor wavelets can be oriented to have excellent selectivity in any desired direction. They respond strongly to image features which are aligned in the same direction and their response to other feature directions is weak. Invariance properties to shifts and rotations also play an important role in their success. In order to accurately capture local features in face images, a space frequency analysis is desirable. Gabor functions provide the best tradeoff between spatial resolution and frequency resolution. The optimal frequency-space localization property allows Gabor wavelets to extract the maximum amount of information from local image regions. This optimal local representation of Gabor wavelets makes them insensitive and robust to facial expression changes in face recognition applications. The representation is also insensitive to illumination variations due to the fact that it lacks the DC component. Last but not least, there is a strong

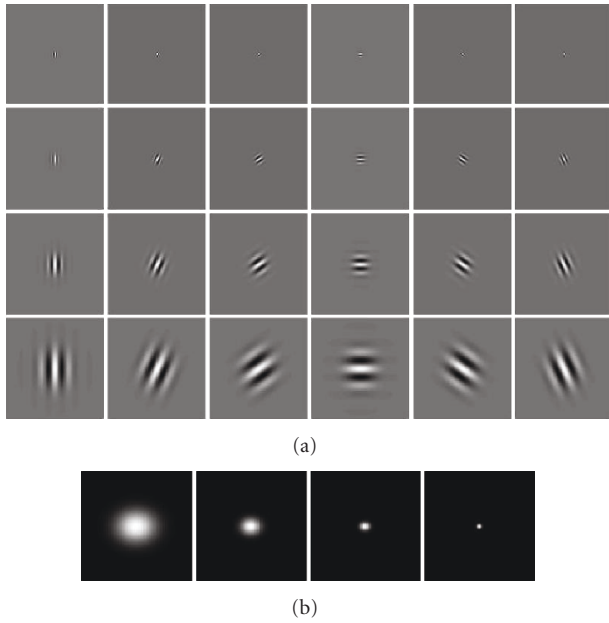


FIGURE 1: Gabor wavelets. (a) The real part of the Gabor kernels at four scales and six orientations. (b) The magnitude of the Gabor kernels at four different scales.

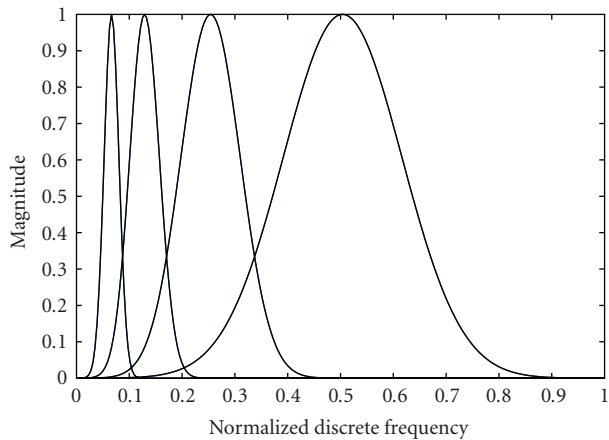


FIGURE 2: Frequency response of 1-dimensional Gabor wavelets ($f = [0.5, 0.25, 0.125, 0.0625]$ and $\eta = 1$).

biological relevance of processing images by Gabor wavelets as they have similar shapes to the respective fields of simple cells in the primary visual cortex.

Figures 3(a) and 3(b) show the magnitude and real part of a Gabor wavelet-transformed face image, where the parameters are $f = [0.5, 0.25, 0.125, 0.0625]$ and $\eta = 1$. Despite many advantages of Gabor wavelet-based algorithms in face recognition, the high-computational complexity and high memory capacity requirement are important disadvantages. With a face image of size 128×128 , the dimension of the extracted Gabor features would be 655 360, when 40 wavelets are used. This feature is formed by concatenating the result of convolving the face image with all the 40 wavelets. Such vector dimensions are extremely large and,

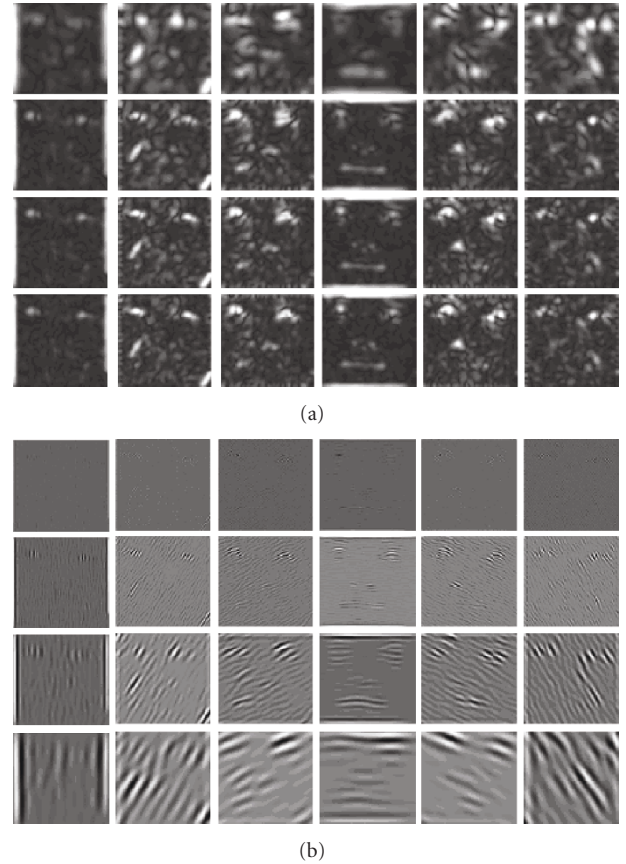


FIGURE 3: Gabor wavelet transformation of a sample image (top left face in Figure 12). (a) The magnitude of the transformation. (b) The real part of the transformation.

in most cases, downsampling is employed before further dimensionality reduction techniques such as PCA is applied. The computational complexity is high even when fast Fourier transform (FFT) is employed.

Because of the above-mentioned shortcomings, one usually looks for other transforms that can preserve most of the desired properties of Gabor wavelets and at the same time reduces the computational complexity and memory requirement. Complex wavelet transforms provide a satisfactory alternative to this problem.

3. COMPLEX WAVELET TRANSFORM

3.1. Dual-tree complex wavelet transform

One of the most promising decompositions that remove the above drawbacks satisfactorily is the dual-tree complex wavelet transform (DT-CWT) [28–31]. Two classical wavelet trees (with real filters) are developed in parallel, with the wavelets forming (approximate) Hilbert pairs. One can then interpret the wavelets in the two trees of the DT-CWT as the real and imaginary parts of some complex wavelet $\Psi_c(t)$. The requirement for the dual-tree setting for forming Hilbert transform pairs is the well-known half-sample delay condition. The resulting complex wavelet is

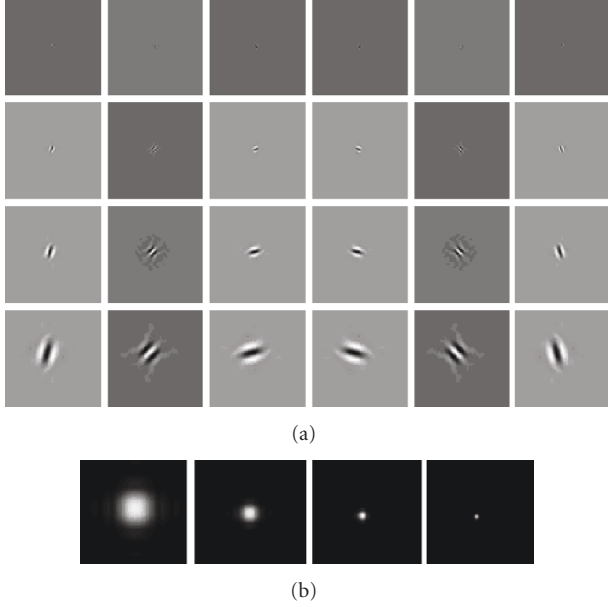


FIGURE 4: Impulse response of dual-tree complex wavelets at 4 levels and 6 directions. (a) Real part. (b) Magnitude.

then approximately analytic (i.e., approximately one sided in the frequency domain). The design of filter banks satisfying the half-sample delay condition can be found in [32–35]. The properties of the DT-CWT can be summarized as

- (i) approximate shift invariance;
- (ii) good directional selectivity in 2 dimensions;
- (iii) phase information;
- (iv) perfect reconstruction using short linear-phase filters;
- (v) limited redundancy, independent of the number of scales, 2 : 1 for 1D ($2m$: 1 for mD);
- (vi) efficient order- N computation—only twice the simple DWT for 1D ($2m$ times for mD).

The transform has the ability to differentiate positive and negative frequencies and produces six subbands oriented in $\pm 15, \pm 45, \pm 75$. However, these directions are fixed unlike the Gabor case, where the wavelets can be oriented in any desired direction.

Figure 4 shows the impulse responses of the dual-tree complex wavelets. It is evident that the transform is selective in 6 directions in all of the scales except the first. Comparing the directional selectivity at different directions using Figures 1 and 4 reveals that the selectivity of the DT-CWT is far from Gabor. Figure 5 shows the frequency responses of the dual-tree complex wavelets at four levels. It is evident that wavelets at first level are not analytic. However, subsequent levels become approximately analytic. The responses depicted for levels above the first level are of bandpass nature, however, their shapes are not Gaussian. Figures 6 shows the magnitude and real part of a face image processed using the DT-CWT.

3.2. Single-tree complex wavelet transform

Complex wavelets with improved analytic property (better suppression of the negative frequencies) are possible in the single-tree context. With improved analyticity property, the wavelets become more selective and respond more strongly to the six-fixed directions of the DT-CWT. Additionally, as a consequence of the improved analyticity, shift invariance property of the wavelets also improves. Thus, it becomes possible to design wavelets which can imitate Gabor wavelets more closely. Complex wavelets with desired properties such as symmetry and orthogonality have been extensively studied in the literature [37–40]. These wavelets, however, are not analytic and thus do not possess the properties associated with analytic wavelets. We now describe the construction of approximately analytic complex wavelet transforms which possess all the properties of the DT-CWT with better directional selectivity and better shift invariance properties. Let the discrete-time complex sequences $h_0(n)$ and $h_1(n)$ denote, respectively, the scaling and wavelet filters of a given multiresolution analysis. They are associated with the scaling function $\phi_h(t)$ and wavelet $\psi_h(t)$ by the following dilation equations:

$$\begin{aligned}\phi_h(t) &= 2 \sum_n h_0(n) \phi(2t - n), \\ \psi_h(t) &= 2 \sum_n h_1(n) \phi(2t - n).\end{aligned}\quad (3)$$

The dual scaling function $\phi_f(t)$ and dual wavelet $\psi_f(t)$ can be defined similarly with sequences $f_0(n)$ and $f_1(n)$. The frequency responses of the scaling function and the wavelet on the analysis side are given, respectively, by the following infinite products:

$$\begin{aligned}\Phi_h(\omega) &= \prod_{k=1}^{\infty} H_0(e^{j\omega/2^k}) \Phi_h(0), \\ \Psi_h(\omega) &= H_1(e^{j\omega/2}) \Phi_h(\omega/2) \\ &= H_1(e^{j\omega/2}) \prod_{k=2}^{\infty} H_0(e^{j\omega/2^k}) \Phi_h(0).\end{aligned}\quad (4)$$

For convergence of the infinite products, one requires $H_0(e^0) = 1$. Without loss of generality, we take $\Phi_h(0) = 1$. The frequency responses of the scaling function and the wavelet on the synthesis side are defined similarly.

In order to achieve an analytic wavelet, one is forced to make the frequency response of the scaling function one sided. Thus, the scaling filter $H_0(e^{j\omega})$ becomes the determining factor for establishing the analyticity of the scaling function and consequently that of the wavelet. The scaling filter can be written in terms of the real and imaginary parts as

$$H_0(e^{j\omega}) = H_0^r(e^{j\omega}) + jH_0^i(e^{j\omega}). \quad (5)$$

Defining the ratio of imaginary and real parts as

$$\Lambda_{H_0}(e^{j\omega}) = \frac{H_0^i(e^{j\omega})}{H_0^r(e^{j\omega})}, \quad (6)$$

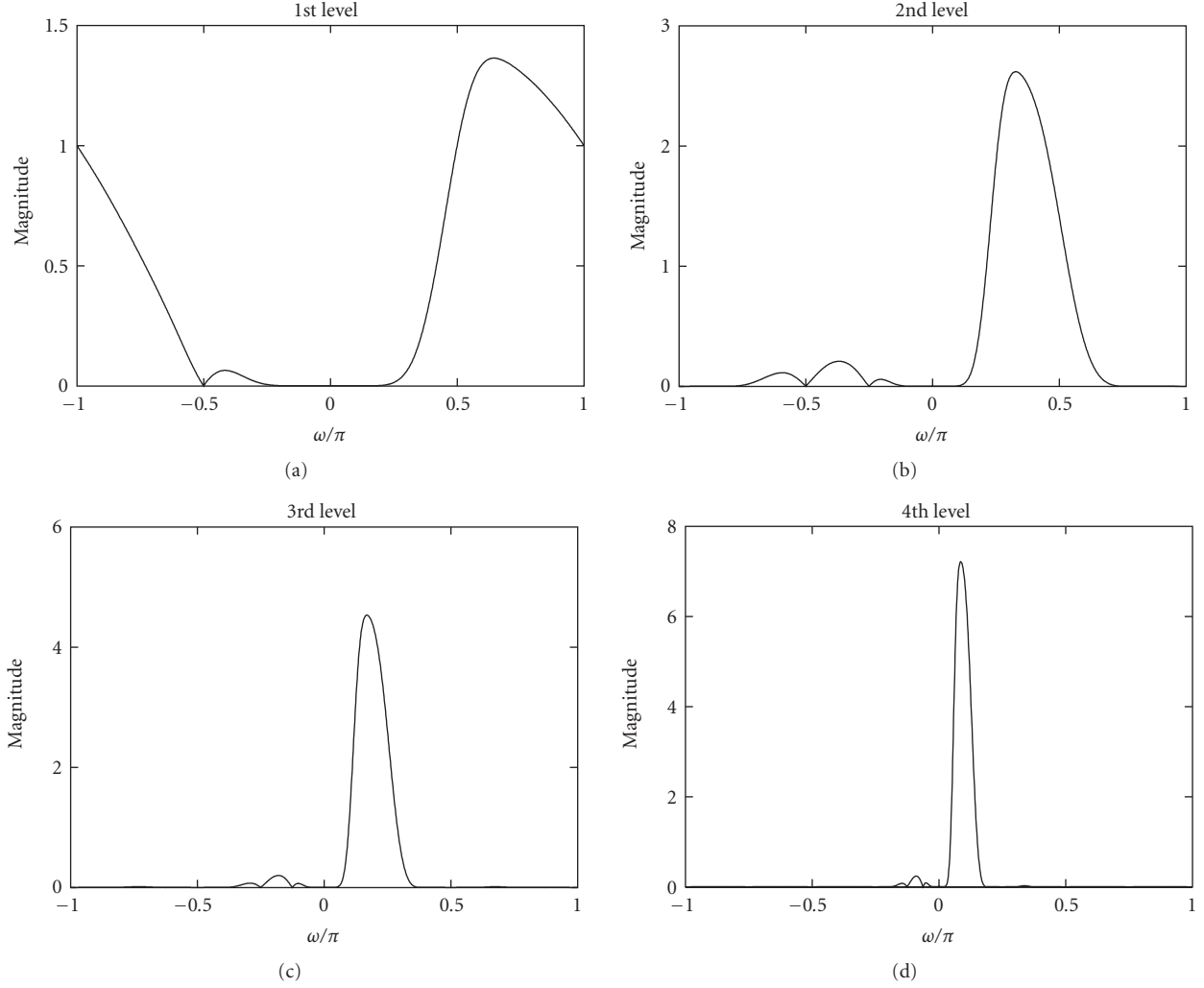


FIGURE 5: Frequency response of 1-dimensional wavelets in the first 4 levels for the DT-CWT (filters in first level are from daubechies “db10” filterbank and subsequent levels are filters from [36]).

the scaling function in (4) can be expressed as

$$\Phi_h(\omega) = \prod_{k=1}^{\infty} H_0^r(e^{j\omega/2^k}) \prod_{k=1}^{\infty} (1 + j\Lambda_{H_0}(e^{j\omega/2^k})). \quad (7)$$

If the scaling filter $H_0(e^{j\omega})$ is analytic, the ratio defined in (6) can be expressed as

$$\Lambda_{H_0}(e^{j\omega}) = e^{-j\sigma(\omega)\pi/2}, \quad \omega \in (-\pi, \pi), \quad (8)$$

where $\sigma(\omega)$ is the signum function (i.e., $\sigma(\omega) = 1$ if $\omega > 0$ and $\sigma(\omega) = -1$ if $\omega < 0$). The analyticity of the scaling filter implies that $1 + j\Lambda_{H_0}(e^{j\omega}) = 0$ for any $\omega \in (-\pi, 0)$. Since for any $\omega < 0$ there exists an integer $L > 0$ such that $\omega/2^k \in (-\pi, 0)$. For $k > L$, it follows that the second infinite product in (7) becomes zero for any $\omega < 0$ rendering $\Phi_h(\omega)$ one sided. Therefore, $\phi_h(t)$ becomes analytic and consequently $\psi_h(t)$ becomes analytic. Analyticity, however, can only be achieved in an approximate sense due to the perfect reconstruction and convergence requirements.

We now consider the design of two-band biorthogonal filter banks which lead to complex biorthogonal wavelet bases that are approximately analytic (see Figure 7). The following setting is adopted for the design.

$$\begin{aligned} \Lambda_{H_0}(e^{j\omega}) &\cong e^{-j\sigma(\omega)\pi/2}, \\ \Lambda_{F_0}(e^{j\omega}) &\cong e^{j\sigma(\omega)\pi/2}, \end{aligned} \quad \omega \in (-\pi, \pi). \quad (9)$$

This implies that the frequency responses of the analysis and synthesis wavelets are zero for negative and positive frequencies, respectively. Phase parts of (9) are satisfied exactly by picking conjugate symmetric filters for both $h_0(n)$ and $f_0(n)$. One then imposes the desired approximation orders K_h and K_f on the analysis and synthesis sides by picking the filters with the following structure:

$$H_0(z) = (1 + z^{-1})^{K_h} Q_h(z), \quad F_0(z) = (1 + z^{-1})^{K_f} Q_f(z), \quad (10)$$

where $Q_h(z)$ and $Q_f(z)$ are arbitrary polynomials.

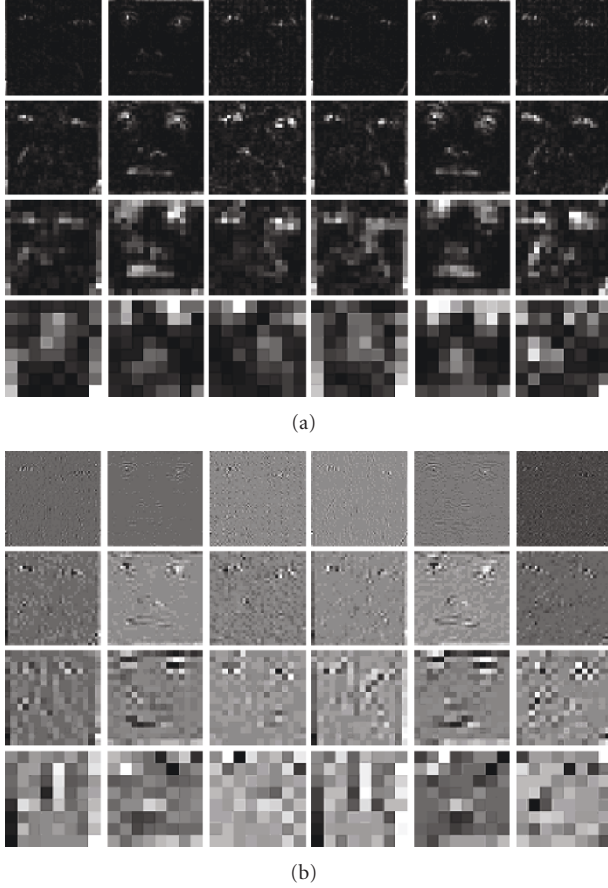


FIGURE 6: DT-CWT transformation of a sample image (top left face in Figure 12). (a) The magnitude of the transformation. (b) The real part of the transformation.

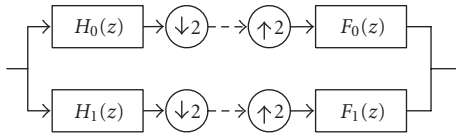


FIGURE 7: Two-band critically downsampled complex biorthogonal filterbank ($H_0(z)$ and $H_1(z)$ are analysis filters; $F_0(z)$ and $F_1(z)$ are synthesis filters).

Let us concentrate on solutions, where the lengths (L) and approximation orders (K_h, K_f) of the analysis and synthesis scaling filters are the same. We further restrict the filter lengths to be minimum, that is, $L = 2K$ thus the approximation orders are forced to be odd.

Since the scaling filters $h_0(n)$ and $f_0(n)$ are conjugate symmetric, the sequences $q_h(n)$ and $q_f(n)$ (which are the inverse z -transforms of $Q_h(z)$ and $Q_f(z)$) are also conjugate symmetric. This implies that the roots of polynomials $Q_h(z)$ and $Q_f(z)$ come in conjugate reciprocal pairs. Note that the halfband filter $P(z) = H_0(z)\tilde{F}_0(z)$ is in general complex. In the case where the halfband filter is real, the sequences $q_h(n)$ and $q_f(n)$ are conjugates of each other. Thus, the roots of $P(z)$ (in addition to the ones at $z = -1$) are of the

TABLE 1: Filter coefficients of conjugate symmetric two-band complex biorthogonal filterbank.

$L = 6, K_h = K_f = 3$ (real halfband filter case, minimum length)	
n	$h_0(n)$
0	$-0.09556007476958 + 0.05086277725442i$
1	$0.08121662052706 + 0.15258833176326i$
2	$0.72145023542907 + 0.10172555450884i$
$L = 10, K_h = K_f = 5$ (real halfband filter case, minimum length)	
n	$h_0(n)$
0	$0.01047379228843 - 0.02059993427869i$
1	$-0.06060208780796 - 0.03081241286301i$
2	$-0.21092863561874 + 0.15493694986530i$
3	$0.10799981987069 + 0.44368598398706i$
4	$0.86016389245414 + 0.2785365553743i$
$L = 8, K_h = K_f = 3$ (real halfband filter case, parameterized)	
n	$h_0(n)$
0	$-0.01538991564970 - 0.04304682801003i$
1	$-0.19237063935158 + 0.06877551842869i$
2	$0.01518588724447 + 0.46460752334624i$
3	$0.89968144894336 + 0.35278517690752i$

TABLE 2: Aliasing energy ratio in dB.

Level	DT-CWT (filter from [30])	ST-CWT (length 10 filters)
Level 1	$-\infty$	$-\infty$
Level 2	-31.40	-33.54
Level 3	-27.93	-31.70
Level 4	-31.13	-32.27

form $\{z_k, 1/z_k^*, z_k^*, 1/z_k\}$. Here, if z_k is a root of $Q_h(z)$, its other root is $1/z_k^*$ and the pair $\{z_k^*, 1/z_k\}$ constitute the roots of $Q_f(z)$. The design looks for filters for which $\Lambda_{H_0}(e^{j\omega})$ and $\Lambda_{F_0}(e^{j\omega})$ have unity magnitude responses subject to the biorthogonality constraint $H_0(z)\tilde{F}_0(z) + H_0(-z)\tilde{F}_0(-z) = 1$ [31]. With the minimum length solutions, there exist no free parameters for optimizing the unity magnitude condition. If one allows $L > 2K$ then the solutions are parameterized and the unity magnitude condition can be optimized.

Table 1 gives half of the coefficients of the low-pass scaling filters. The first two filters correspond to minimum length solutions with length $L = 6, K = 3$, and $L = 10, K = 5$, where the third filter is a nonminimum length solution with $L = 8, K = 3$.

Figure 8 shows the impulse response of the ST-CWT. Similar to the DT-CWT, the ST-CWT is selective in 6 directions. Comparing Figures 1, 4, and 8, the selectivity of ST-CWT is almost like that of Gabor. In order to assess the shift invariant property of the ST-CWT and compare it with DT-CWT, we use the aliasing energy ratio introduced by Kingsbury [30].

Table 2 clearly indicates that the energy aliasing ratio for the ST-CWT is better with more than 1 dB for all levels when compared to that of DT-CWT.

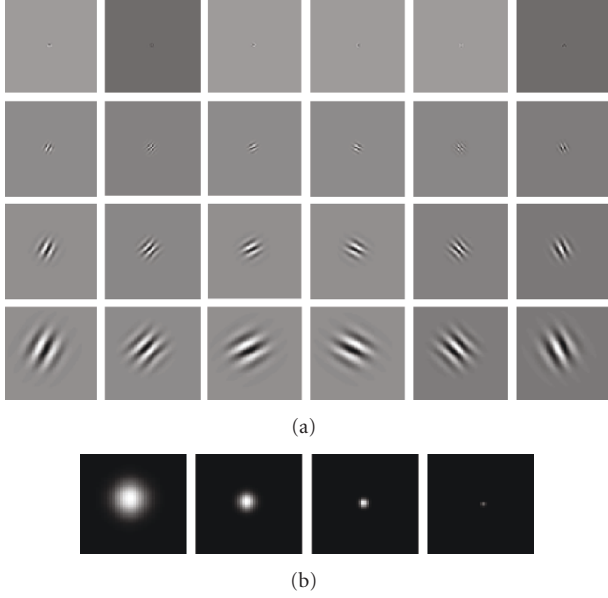


FIGURE 8: Impulse response of single-tree complex wavelet at 4 levels and 6 directions. (a) Real part. (b) Magnitude.

Figure 9 shows the frequency responses of the single-tree complex wavelets at four levels. The wavelets at first level are not analytic. However, subsequent levels become approximately analytic. The responses depicted for levels above the first level are of bandpass nature and they better approximate a Gaussian shape. Figure 10 shows the magnitude and real part of a face image processed using the ST-CWT.

4. PROPOSED METHOD

In order to alleviate the computational burden and high memory requirement of the Gabor wavelet-based face recognition, and at the same time retain most of its desired properties, we propose to use complex approximately analytic wavelets instead of Gabor wavelets. We specifically consider two alternatives; the complex dual-tree wavelet transform and the complex single-tree wavelet transform described in Section 3. For both approaches, the directional multiscales decomposition of the gray level face image are performed up to level 4. The DT-CWT or ST-CWT feature vector X is formed by concatenating the results of the multiscale representation. Given an image $I(x, y)$ and a wavelet $\psi_{\mu, \nu}(x, y)$, of level μ and direction ν , vector X can be formed by

$$X = (O_{0,0} \ O_{0,1} \ \cdots \ O_{3,5})^t, \quad (11)$$

where $Q_{\mu, \nu}(x, y) = I(x, y) * \psi_{\mu, \nu}(x, y)$ and $Q_{\mu, \nu} \mu = 0, \dots, 3$, $\nu = 0, 1, \dots, 5$ is formed by concatenating the rows or columns of $Q_{\mu, \nu}(x, y)$. Here, $*$ and t denote the convolution and transpose operators, respectively. This representation encompasses different scales, spatial location, and 6-fixed orientations similar to Gabor representation.

The size of such a feature vector is 32640 pixels which is much smaller than the corresponding Gabor feature vector where the size is 393216. For the Gabor setting, we employed downsampling factor of 4, 16, and 32 in order to reduce the dimensionality of the feature vector to manageable sizes. For the complex wavelets, due to the intrinsic downsampling of the multiscale transform, we employed an extradyadic downsampling strategy to further reduce the size of the feature vector. The feature vectors even after downsampling are of very high dimension and therefore not very convenient to be used directly for recognition. To reduce the dimensionality of the feature vector space, we employed PCA on the Gabor, DT-CWT, and ST-CWT feature vectors. Figure 11 shows the block diagram of the proposed method.

The similarity measures used in our experiments to evaluate the efficiency of different representation and recognition methods include L_1 distance measure, δ_{L1} , L_2 distance measure, δ_{L2} , and cosine similarity measure, δ_{\cos} . The measures for n dimensional vectors are defined as follows [41]:

$$\begin{aligned} \delta_{L1}(x, y) &= \|x - y\| = \sum_{i=1}^n |x_i - y_i|, \\ \delta_{L2}(x, y) &= \|x - y\|^2 = \sqrt{\sum_{i=1}^n (x_i - y_i)^2}, \\ \delta_{\cos}(x, y) &= -\frac{x \cdot y}{\|x\| \|y\|} = -\frac{\sum_{i=1}^n x_i y_i}{\sqrt{\sum_{i=1}^n x_i^2} \sqrt{\sum_{i=1}^n y_i^2}}. \end{aligned} \quad (12)$$

We conducted experiments on two commonly used face databases: FERET database [42] and ORL database [43]. For FERET database, 600 frontal face images from 200 subjects are selected, where all the subjects are in an upright, frontal position. The 600 face images were acquired under varying illumination conditions and facial expressions. Each subject has three images of size 256×384 with 256 gray levels. The following procedures were applied to normalize the face images prior to the experiments:

- (i) each face image is cropped to the size of 128×128 to extract the facial region using the algorithm in [44],
- (ii) each face image is normalized to zero mean and unit variance.

Figure 12 shows sample images from the database. The first two rows are the example training images while the third row shows the example test images. It can be seen from this figure that the test images all display variations in illumination and facial expression.

To test the algorithms, two images of each subject are randomly chosen for training, while the remaining one is used for testing (i.e., 400 training and 200 test images).

The ORL database consists of 400 images acquired from 40 persons (i.e., ten different images of each of 40 distinct subjects of both genders) taken over a period of two years with variations in facial expression and facial details. All images were taken under a dark background and the subjects

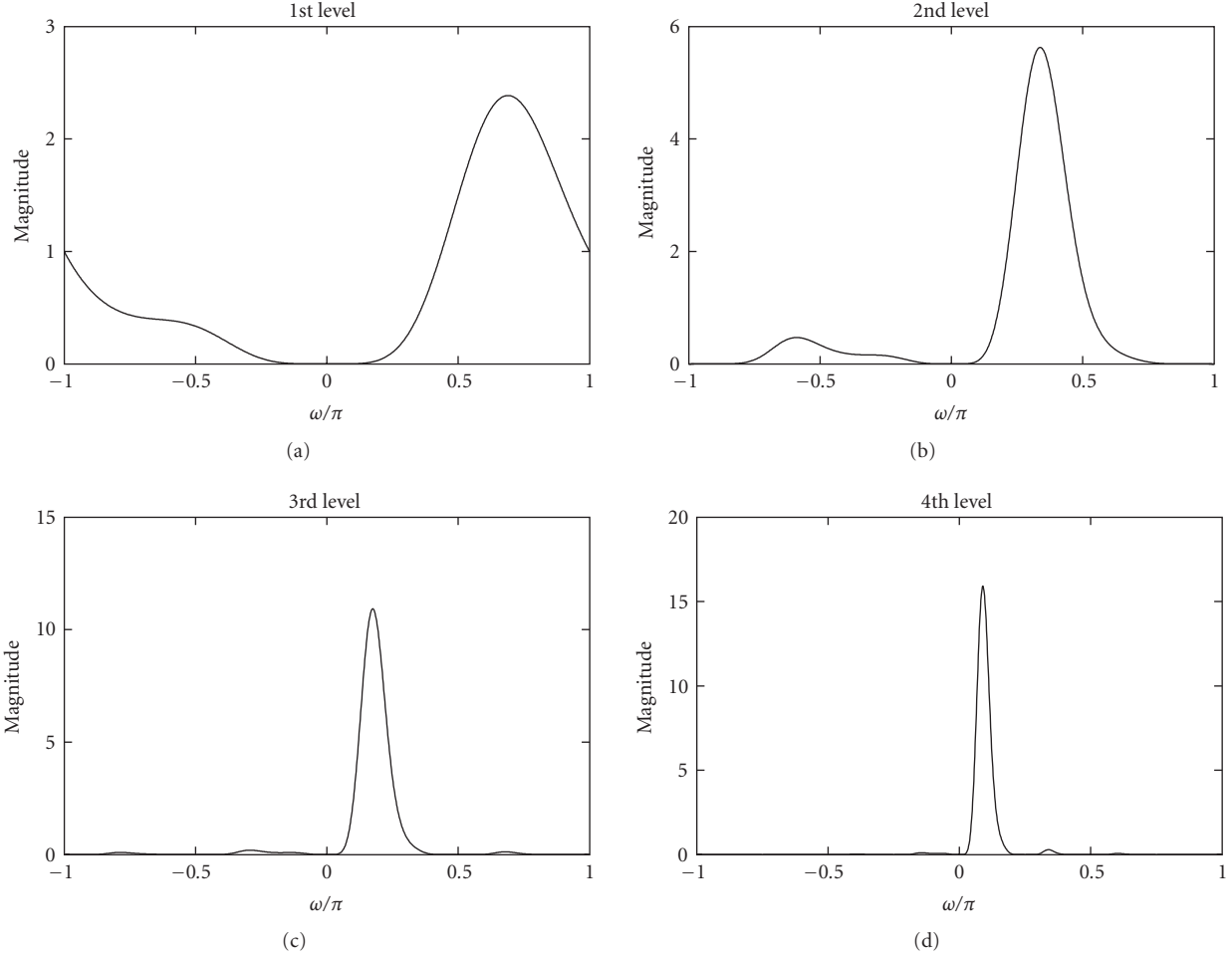


FIGURE 9: Frequency response of 1-dimensional wavelets in the first 4 levels for the ST-CWT (length 10 complex filters from Table 1).

were in an upright frontal position with tilting and rotation tolerance up to 20 degree and tolerance of up to about 10% scale. All images are grey scale with a 92×112 pixels resolution. All images in the database are resized to 128×128 pixels for our experiments.

Out of the 10 images per subject of the ORL face database, the first 5 were selected for training and the remaining 5 were used for testing (i.e., 200 training and 200 test images). Hence, no overlap exists between the training and test face images. Figure 13 shows sample images from the database.

5. SIMULATION RESULTS AND DISCUSSIONS

In order to compare and assess the discriminating power of the complex wavelet-based representations, we first obtain the Gabor, DT-CWT, and ST-CWT features and use the L_1 , L_2 , and cos distance measures to classify the face images without any dimensionality reduction. The results are given in Tables 3 and 4 for the Gabor, DT-CWT, and ST-CWT, respectively, using the FERET face database. The superscripts on the feature vector indicate the downsampling factors employed. Note that for the complex wavelet-based

TABLE 3: Face recognition performance for Gabor wavelets with different downsampling factors using FERET database and three different similarity measures: L_1 distance measure, δ_{L_1} , L_2 distance measure, δ_{L_2} and cosine similarity measure, δ_{\cos} .

Gabor	dim	δ_{L_1}	δ_{L_2}	δ_{\cos}
$X^{(1)}$	393216	93.83	91.67	91.67
$X^{(4)}$	98304	93.5	91.17	91.17
$X^{(16)}$	24576	92.5	89.5	89.5
$X^{(32)}$	12288	88.33	84.67	84.67

representation, we employed a downsampling strategy that is scale dependent unlike the Gabor representation, where the downsampling strategy is independent of the scale. The numbers on the superscript refer, in order, to the downsampling factors from the first to fourth scales. The resulting dimension of the feature vector after downsampling is also indicated in the second column of the respective tables.

The results clearly indicate that the complex wavelet-based representation is as discriminating as the Gabor-based representation. When no downsampling is employed,

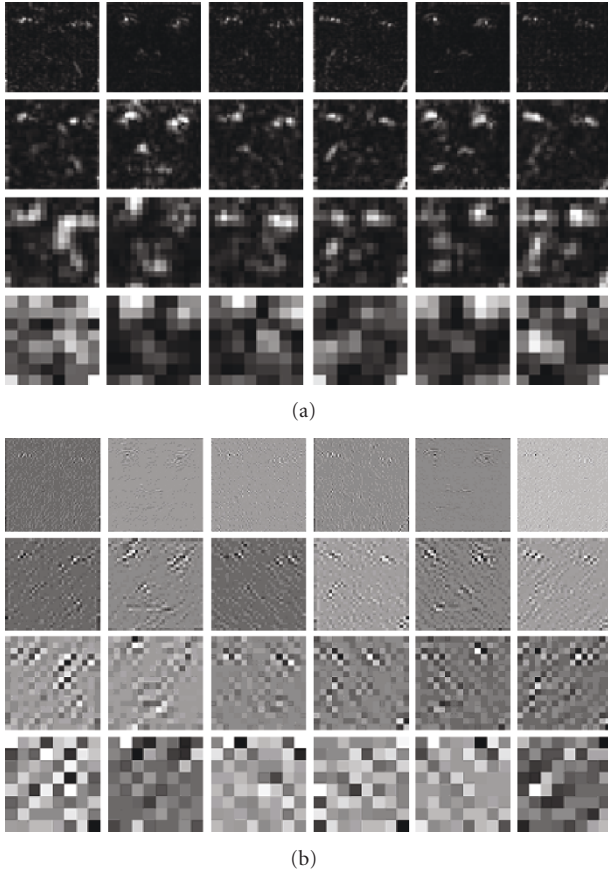


FIGURE 10: ST-CWT transformation of a sample image (top left face in Figure 12). (a) The magnitude of the transformation. (b) The real part of the transformation.

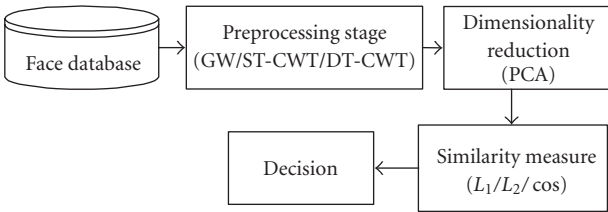


FIGURE 11: The block diagram of the proposed method.

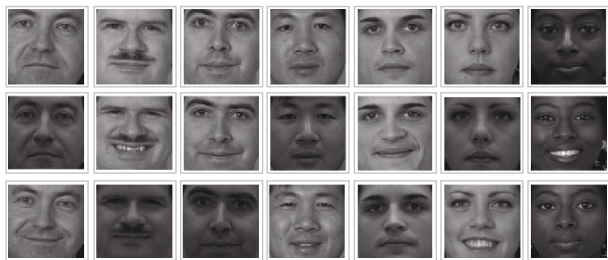


FIGURE 12: Example FERET images used in our experiments (cropped to the size of 128×128 to extract the facial region). The figure shows in the top two rows the examples of training images used in our experiments and in the bottom row the examples of test images.



FIGURE 13: Example ORL images used in our experiments (resized to 128×128). The figure shows two subject images, where the first 2 rows used for training and the second 2 rows used for testing.

TABLE 4: Face recognition performance for DT-CWT and ST-CWT with different downsampling factors using FERET database and three different similarity measures: L_1 distance measure, δ_{L_1} , L_2 distance measure, δ_{L_2} and cosine similarity measure, δ_{\cos} .

DT-CWT / ST-CWT dim	δ_{L_1}	δ_{L_2}	δ_{\cos}
$X^{(1\ 1\ 1\ 1)}$	92.83/93.33	89.83/91.83	91.17/92.00
$X^{(4\ 2\ 1\ 1)}$	94.00/93.17	90.17/91.83	91.33/91.67
$X^{(8\ 4\ 2\ 1)}$	93.00/92.33	88.67/90.00	89.67/90.17
$X^{(16\ 8\ 4\ 2)}$	93.17/90.50	87.50/87.33	86.00/87.17

the Gabor features give 93.83% recognition whereas DT-CWT and ST-CWT give, respectively, 92.83% and 93.33% recognition rates when L_1 distance measure is used. It should be noted that with no downsampling, the dimension of the Gabor feature vector is approximately twelve times that of DT-CWT or ST-CWT. The same conclusion holds even when the downsampling factors are high such that the recognition uses less number of features. With 2880 features, the recognition rates of DT-CWT and ST-CWT are over 90%, where that of Gabor with 12288 features falls to 88.33% when L_1 distance measure is used. Similar observations can be made for the other two distance measures considered. Thus, it can be concluded that complex wavelet-based representations provide robust signatures for the face recognition problem. Furthermore, a comparison between the two complex wavelet transforms reveals that their recognition rates are similar with the DT-CWT being slightly better for higher downsampling factors for the L_1 distance measure, whereas the ST-CWT is slightly better for the L_2 and cos distance measures.

We next use the derived features together with PCA as a dimensionality reduction technique to assess the performance of the complex wavelet-based representations.

Figures 14 and 15 show the face recognition performance of PCA, Gabor+PCA, DT-CWT+PCA, and ST-CWT+PCA

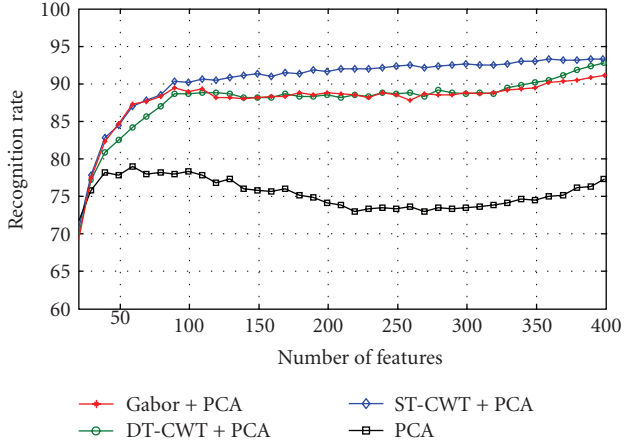


FIGURE 14: Face recognition performance of the FERET database using PCA, Gabor+PCA, DT-CWT+PCA, and ST-CWT+PCA for the $\delta_{L_1}(L_1)$ similarity measure. The recognition rate means the accuracy rate for the top response being correct.

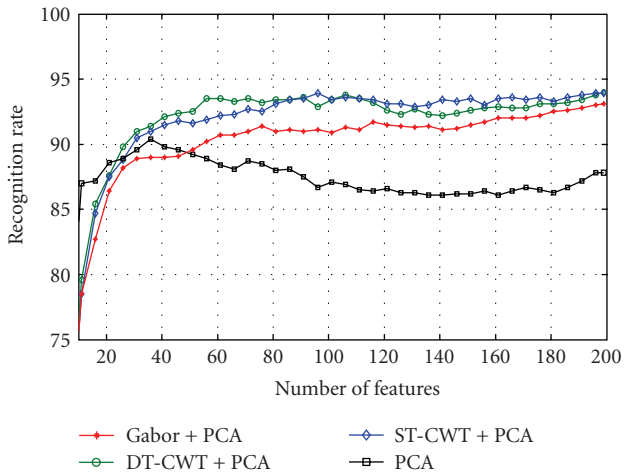


FIGURE 15: Face recognition performance of the ORL database using PCA, Gabor+PCA, DT-CWT+PCA, and ST-CWT+PCA for the $\delta_{L_1}(L_1)$ similarity measure. The recognition rate means that the accuracy rate for the top response is correct.

for the $\delta_{L_1}(L_1)$ similarity measure using the FERET and ORL databases, respectively. For the FERET database, PCA applied on raw face images recorded a recognition rate which was always less than 79%. The performances of the Gabor+PCA, DT-CWT+PCA, and ST-CWT+PCA are significantly better than that of raw PCA. With 100 features, the performance of ST-CWT+PCA is just over 90%, where Gabor+PCA and DT-CWT+PCA perform just under 89%. When 200 features are employed, the recognition rates for Gabor+PCA, DT-CWT+PCA, and ST-CWT+PCA are, respectively, 88.83%, 88.5%, and 91.67%. These results indicate that CWT-based features are not as sensitive as PCA to illumination variations and facial expression changes.

Table 5 summarizes the results for the FERET database for all the distance measures considered in this paper when

TABLE 5: Face recognition performance for different approaches using 200/400 features and FERET database with three different similarity measures.

Approach	δ_{L_1}	δ_{L_2}	δ_{\cos}
PCA	74.17/77.33	78.0/78.17	78.33/78.5
Gabor+PCA	88.83/92.83	89.67/91.17	90.0/91.17
DT-CWT+PCA	88.50/93.0	87.67/89.83	90.5/91.17
ST-CWT+PCA	91.67/93.33	91.5/91.83	91.17/92.0

TABLE 6: Face recognition performance for different approaches using 100/200 features and ORL database with three different similarity measures.

Approach	δ_{L_1}	δ_{L_2}	δ_{\cos}
PCA	87.33/88.25	90.0/91.0	91.92/91.75
Gabor+PCA	91.17/93.1	91.33/92.5	93.25/93.59
DT-CWT+PCA	93.59/94.1	94.0/94.0	94.50/94.75
ST-CWT+PCA	93.83/94.59	93.41/94.33	94.67/94.92

200 and 400 features are used. We conclude that complex wavelet representation-based face recognition performs slightly better than Gabor+PCA and the ST-CWT+PCA does slightly better than DT-CWT+PCA.

Similar results hold for the ORL database. PCA applied on raw face images recorded a recognition rate which was always less than 90%. The performances of the Gabor+PCA, DT-CWT+PCA, and ST-CWT+PCA are again significantly better than that of raw PCA. With 100 features, the performances of ST-CWT+PCA and DT-CWT+PCA are close to each other with 93.83% and 93.59%, respectively, where Gabor+PCA performed slightly worse at 91.17%. When all features are employed, the recognition rates for Gabor+PCA, DT-CWT+PCA, and ST-CWT+PCA are, respectively, 93.1%, 94.1%, and 94.59% with L_1 as the distance measure.

Table 6 summarizes the results for the ORL database when 100 and 200 features are used. We again can conclude that complex wavelet representation-based face recognition performs slightly better than Gabor, and the ST-CWT does slightly better than DT-CWT.

6. COMPUTATIONAL COMPLEXITY ANALYSIS FOR FEATURE EXTRACTION

In this section, we will analyze and compare the computational complexity of extracting features using Gabor wavelets and complex wavelets. Computations refer to the number of real additions and real multiplications required for extracting the features of an image. In our analysis, we assume that the image size is a power of 2 so that the fast Fourier transform (FFT) can be applied when using Gabor for faster feature extraction.

Given an $N \times N$ image and a Gabor wavelet with an arbitrary scale and orientation, Gabor wavelet features are extracted by convolution. The convolution is implemented by using the FFT, then point-by-point multiplications in

TABLE 7: Computational complexity analysis of feature extraction using Gabor wavelets, DT-CWT and ST-CWT (N^2 : total images pixels).

Approach	+	×
Gabor wavelets	$SD(6N^2\log_2N^2+2N^2)$	$SD(4N^2\log_2N^2+4N^2)$
Complex wavelets	$(32/3)N^2L + 2N^2$	$(32/3)N^2L$
Gain factor : ($S = 4$, $D = 6, L = 10, N = 128$)	18.99	13.5

the frequency domain, and finally the inverse FFT (IFFT). Assume that the FFTs of the Gabor wavelets are precomputed. The FFT of an $N \times N$ image requires $N^2\log_2N^2$ complex additions and $0.5N^2\log_2N^2$ complex multiplications. The IFFT requires the same amount of computation as the FFT. The point-by-point multiplications involve N^2 complex multiplications. Performing one complex addition requires 2 real additions, while one complex multiplication requires 2 real additions and 4 real multiplications. Therefore, feature extraction based on Gabor wavelets requires a total of $2N^2\log_2N^2$ complex additions and $N^2\log_2N^2 + N^2$ complex multiplications; this is equivalent to a total of $6N^2\log_2N^2 + 2N^2$ real additions and $4N^2\log_2N^2 + 4N^2$ real multiplications. For S scales and D directions, one requires $SD(6N^2\log_2N^2 + 2N^2)$ real additions and $SD(4N^2\log_2N^2 + 4N^2)$ real multiplications.

The DT-CWT and ST-CWT have similar computational complexities and it is equivalent to implementing 2 real DWTs. Due to the downsampling by 2, the complexity goes down by a factor of 2 for each successive scale in 1 dimension and by a factor of 4 in 2 dimensions. Assuming that the 1-dimensional filters implementing the complex wavelet transform is of length L , in the first level, we have $8N^2(L - 1)$ real additions and $8N^2L$ real multiplications. Thus, for a complex wavelet transform with S scales, one has $(32/3)N^2(L - 1)(1 - (1/4)^S)$ real additions and $(32/3)N^2L(1 - (1/4)^S)$ real multiplications. For a scale $S > 3$, the total real additions and real multiplications can, respectively, be approximated as $(32/3)N^2L$ and $(32/3)N^2L$. The last piece of computation is the addition and subtraction of respective subbands to create the six directional complex wavelets in each scale. The real additions required for this task are $2N^2$. Thus, the complex wavelet implementation requires $(32/3)N^2L + 2N^2$ real additions and $(32/3)N^2L$ real multiplications. Thus, compared to Gabor wavelets, for a face image of size 128×128 , a filter of length 10 and a multiscale representation with 4 scales and 6 directions, the number of real additions and real multiplications is reduced by factors of 18.99 and 13.5, respectively. This reduction becomes more significant for larger image sizes and more scales. Table 7 summarizes the results of computational complexity analysis.

7. CONCLUSIONS

Complex wavelets possess most of the properties of Gabor wavelets such as good directional selectivity and invariance to shifts and in-plane rotations and a representation that is

local. They, however, have important advantages: they are computationally much more efficient and enjoy a much less redundant representation.

In this paper, we first constructed filters for an approximately analytic complex wavelet transform in the single-tree context with good directional selectivity and invariance to shifts and in-plane rotations much like the Gabor wavelets. We then systematically investigated the representation and discrimination power of newly designed wavelets and the recently developed dual-tree complex wavelets for the face recognition problem. The resulting complex wavelet-based feature vectors are as discriminating as the Gabor wavelet derived features. This conclusion holds even when the feature vectors are downsampled.

PCA is employed to further reduce the dimensionality of the complex wavelet-based feature space. Extensive experiments are carried out on standard databases. In all experiments, complex wavelets performed equally well or suppressed the performance of Gabor wavelets in recognition rate when equal number of orientations and scales is used. With 6 orientations and 4 scales, the performances of Gabor+PCA, DT-CWT+PCA, and ST-CWT+PCA were 92.83%, 93.0%, and 93.33% for the FERET database and 93.1%, 94.1%, and 94.59% for the ORL database when L_1 distance measure was used. This finding indicates that complex wavelets can provide a successful alternative to Gabor wavelets for face recognition. Furthermore, our experiments indicate that ST-CWT performs slightly better than DT-CWT due to the fact that it has improved directional selectivity and shift invariance properties.

REFERENCES

- [1] R. Chellappa, C. L. Wilson, and S. Sirohey, "Human and machine recognition of faces: a survey," *Proceedings of the IEEE*, vol. 83, no. 5, pp. 705–741, 1995.
- [2] M. Turk and A. Pentland, "Eigenfaces for recognition," *Journal of Cognitive Neuroscience*, vol. 3, no. 1, pp. 71–86, 1991.
- [3] M. Kirby and L. Sirovich, "Application of the Karhunen-Loeve procedure for the characterization of human faces," *IEEE Transactions on Pattern Analysis and Machine Intelligence*, vol. 12, no. 1, pp. 103–108, 1990.
- [4] H. Moon and P. J. Phillips, "Computational and performance aspects of PCA-based face-recognition algorithms," *Perception*, vol. 30, no. 3, pp. 303–321, 2001.
- [5] P. Nicholl and A. Amira, "DWT/PCA face recognition using automatic coefficient selection," in *Proceedings of the 4th IEEE International Workshop on Electronic Design, Test and Applications (DELTA '08)*, pp. 390–393, Hong Kong, January 2008.
- [6] L. Shen, Z. Ji, L. Bai, and C. Xu, "DWT based HMM for face recognition," *Journal of Electronics*, vol. 24, no. 6, pp. 835–837, 2007.
- [7] A. Manjunath, R. Chellappa, and C. von der Malsburg, "A feature based approach to face recognition," in *Proceedings of the IEEE Computer Society Conference on Computer Vision and Pattern Recognition (CVPR '92)*, pp. 373–378, Champaign, Ill, USA, June 1992.
- [8] L. Shen, L. Bai, and M. Fairhurst, "Gabor wavelets and general discriminant analysis for face identification and verification," *Image and Vision Computing*, vol. 25, no. 5, pp. 553–563, 2007.

- [9] O. Pichler, A. Teuner, and B. J. Hosticka, "A comparison of texture feature extraction using adaptive Gabor filtering, pyramidal and tree structured wavelet transforms," *Pattern Recognition*, vol. 29, no. 5, pp. 733–742, 1996.
- [10] C.-J. Lee and S.-D. Wang, "Fingerprint feature extraction using Gabor filters," *Electronics Letters*, vol. 35, no. 4, pp. 288–290, 1999.
- [11] X. Wang, X. Ding, and C. Liu, "Optimized Gabor filter based feature extraction for character recognition," in *Proceedings of the 16th International Conference on Pattern Recognition (ICPR '02)*, vol. 4, pp. 223–226, Quebec, Canada, August 2002.
- [12] M. Lades, J. C. Vorbruegggen, J. Buhmann, et al., "Distortion invariant object recognition in the dynamic link architecture," *IEEE Transactions on Computers*, vol. 42, no. 3, pp. 300–311, 1993.
- [13] L. Wiskott, J.-M. Fellous, N. Kruger, and C. von der Malsburg, "Face recognition by elastic bunch graph matching," *IEEE Transactions on Pattern Analysis and Machine Intelligence*, vol. 19, no. 7, pp. 775–779, 1997.
- [14] B. Zhang, S. Shan, X. Chen, and W. Gao, "Histogram of Gabor phase patterns (HGPP): a novel object representation approach for face recognition," *IEEE Transactions on Image Processing*, vol. 16, no. 1, pp. 57–68, 2007.
- [15] D.-H. Liu, K.-M. Lam, and L.-S. Shen, "Optimal sampling of Gabor features for face recognition," *Pattern Recognition Letters*, vol. 25, no. 2, pp. 267–276, 2004.
- [16] C. Liu and H. Wechsler, "Independent component analysis of Gabor features for face recognition," *IEEE Transactions on Neural Networks*, vol. 14, no. 4, pp. 919–928, 2003.
- [17] M. S. Bartlett, J. R. Movellan, and T. J. Sejnowski, "Face recognition by independent component analysis," *IEEE Transactions on Neural Networks*, vol. 13, no. 6, pp. 1450–1464, 2002.
- [18] S. Shan, W. Gao, Y. Chang, B. Cao, and P. Yang, "Review the strength of Gabor features for face recognition from the angle of its robustness to mis-alignment," in *Proceedings of the 17th International Conference on Pattern Recognition (ICPR '04)*, vol. 1, pp. 338–341, Cambridge, UK, August 2004.
- [19] J.-K. Kamarainen, V. Kyrki, and H. Kälviäinen, "Invariance properties of Gabor filter-based features—overview and applications," *IEEE Transactions on Image Processing*, vol. 15, no. 5, pp. 1088–1099, 2006.
- [20] L. Shen and L. Bai, "A review on Gabor wavelets for face recognition," *Pattern Analysis and Applications*, vol. 9, no. 2–3, pp. 273–292, 2006.
- [21] L. Nanni and D. Maio, "Weighted sub-Gabor for face recognition," *Pattern Recognition Letters*, vol. 28, no. 4, pp. 487–492, 2007.
- [22] W.-P. Choi, S.-H. Tse, K.-W. Wong, and K.-M. Lam, "Simplified Gabor wavelets for human face recognition," *Pattern Recognition*, vol. 41, no. 3, pp. 1186–1199, 2008.
- [23] H. E. Sankaran, A. P. Gotchev, K. O. Egiazarian, and J. T. Astola, "Complex wavelets versus Gabor wavelets for facial feature extraction: a comparative study," in *Image Processing: Algorithms and Systems IV*, vol. 5672 of *Proceedings of SPIE*, pp. 407–415, San Jose, Calif, USA, January 2005.
- [24] T. Celik, H. Özkaramanli, and H. Demirel, "Facial feature extraction using complex dual-tree wavelet transform," *Computer Vision and Image Understanding*, vol. 111, no. 2, pp. 229–246, 2008.
- [25] Y. Sun and M. Du, "Face detection using DT-CWT on SHPCA space," in *Proceedings of the 6th International Conference on Intelligent Systems Design and Applications (ISDA '06)*, vol. 2, pp. 433–437, Jinan, China, October 2006.
- [26] Y. Sun and M. Du, "DT-CWT feature based classification using orthogonal neighborhood preserving projections for face recognition," in *Proceedings of the International Conference on Computational Intelligence and Security (CIS '06)*, pp. 719–724, Guangzhou, China, November 2006.
- [27] Y. Sun, "DT-CWT feature based face recognition using supervised kernel ONPP," in *Proceedings of the International Conference on Computational Intelligence and Security Workshops (CISW '07)*, pp. 312–315, Harbin, China, December 2007.
- [28] N. G. Kingsbury, "The dual-tree complex wavelet transform: a new efficient tool for image restoration and enhancement," in *Proceedings of the 9th European Signal Processing Conference (EUSIPCO '98)*, pp. 319–322, Island of Rhodes, Greece, September 1998.
- [29] N. G. Kingsbury, "Shift invariant properties of the dual-tree complex wavelet transform," in *Proceedings of the IEEE International Conference on Acoustics, Speech, and Signal Processing (ICASSP '99)*, vol. 3, pp. 1221–1224, Phoenix, Ariz, USA, March 1999.
- [30] N. G. Kingsbury, "Complex wavelets for shift invariant analysis and filtering of signals," *Applied and Computational Harmonic Analysis*, vol. 10, no. 3, pp. 234–253, 2001.
- [31] I. W. Selesnick, R. G. Baraniuk, and N. G. Kingsbury, "The dual-tree complex wavelet transform—a coherent framework for multiscale signal and image processing," *IEEE Signal Processing Magazine*, vol. 22, no. 6, pp. 123–151, 2005.
- [32] I. W. Selesnick, "The design of approximate Hilbert transform pairs of wavelet bases," *IEEE Transactions on Signal Processing*, vol. 50, no. 5, pp. 1144–1152, 2002.
- [33] R. Yu and H. Özkaramanli, "Hilbert transform pairs of biorthogonal wavelet bases," *IEEE Transactions on Signal Processing*, vol. 54, no. 6, part 1, pp. 2119–2125, 2006.
- [34] N. G. Kingsbury, "Design of Q-shift complex wavelets for image processing using frequency domain energy minimization," in *Proceedings of the IEEE International Conference on Image Processing (ICIP '03)*, vol. 1, pp. 1013–1016, Barcelona, Spain, September 2003.
- [35] D. B. H. Tay and M. Palaniswami, "Design of approximate Hilbert transform pair of wavelets with exact symmetry," in *Proceedings of the IEEE International Conference on Acoustics, Speech and Signal Processing (ICASSP '04)*, vol. 2, pp. 921–924, Montreal, Canada, May 2004.
- [36] A. F. Abdelnour and I. W. Selesnick, "Design of 2-band orthogonal near-symmetric CQF," in *Proceedings of the IEEE International Conference on Acoustics, Speech, and Signal Processing (ICASSP '01)*, vol. 6, pp. 3693–3696, Salt Lake City, Utah, USA, May 2001.
- [37] B. Belzer, J.-M. Lina, and J. Villasenor, "Complex, linear-phase filters for efficient image coding," *IEEE Transactions on Signal Processing*, vol. 43, no. 10, pp. 2425–2427, 1995.
- [38] X.-P. Zhang, M. D. Desai, and Y.-N. Peng, "Orthogonal complex filter banks and wavelets: some properties and design," *IEEE Transactions on Signal Processing*, vol. 47, no. 4, pp. 1039–1048, 1999.
- [39] X. Q. Gao, T. Q. Nguyen, and G. Strang, "A study of two-channel complex-valued filterbanks and wavelets with orthogonality and symmetry properties," *IEEE Transactions on Signal Processing*, vol. 50, no. 4, pp. 824–833, 2002.
- [40] J.-M. Lina and M. Mayrand, "Complex Daubechies wavelets," *Applied and Computational Harmonic Analysis*, vol. 2, no. 3, pp. 219–229, 1995.

-
- [41] V. Perlibakas, "Distance measures for PCA-based face recognition," *Pattern Recognition Letters*, vol. 25, no. 6, pp. 711–724, 2004.
 - [42] P. J. Philipps, H. Moon, S. Rivzi, and P. Ross, "The FERET evaluation methodology fro face-recognition algorithms," *IEEE Transaction on Pattern Analysis and Machine Intelligence*, vol. 22, no. 10, pp. 1090–1100, 2000.
 - [43] F. Samaria and A. Harter, "Parameterization of a stochastic model for human face identification," in *Proceedings of the 2nd IEEE Workshop on Applications of Computer Vision (WACV '94)*, pp. 138–142, Sarasota, Fla,USA, December 1994.
 - [44] M. Nilsson, J. Nordberg, and I. Claesson, "Face detection using local SMQT features and split up snow classifier," in *Proceedings of the IEEE International Conference on Acoustics, Speech and Signal Processing (ICASSP '07)*, vol. 2, pp. 589–592, Honolulu, Hawaii, USA, April 2007.